Pergamon

Solid State Communications, Vol. 108, No. 6, pp. 343–348, 1998

0038–1098/98 $ - see front matter

PII: S0038–1098(98)00390-1

SPIN-POLARIZED X-RAY EMISSION SPECTROSCOPY OF CAPPED THIN Co FILMS ON Cu(100)

U. Pustogowa [a], L. Szunyogh [a,b], H. Ebert [c] and P. Weinberger [a,d,*]

[a] Center for Computational Materials Science, Gumpendorfer Str. 1a, A-1060 Vienna, Austria

[b] Department of Theoretical Physics, Technical University Budapest, Budafoki út 8, H-1521, Budapest, Hungary

[c] Institut für Physikalische Chemie, Universität München, Theresienstr. 37-41, D-80333 München, Germany

[d] Institut für Technische Elektrochemie, Technische Universität Wien, Getreidemarkt 9/158, A-1060 Vienna, Austria

(*Received* 23 *July* 1998; *accepted* 12 *August* 1998 *by P. Dederichs*)

The theory of valence band X-ray emission spectroscopy (XES) is discussed in terms of spin-polarized fully relativistic multiple scattering. In comparison to the non spin-polarized case new theoretical features are presented with particular emphasis on the dependence of the intensity on the polarization of the emitted photon. Applications to the L_3 XES of a Co monolayer on Cu(100) substrate as capped by a monolayer of various $3d$, $4d$, and $5d$ transition metals are shown since such overlayer systems display systematic variations of the magnetic moment in the Co layer as well as in the cap layer. These changes are clearly mapped in the calculated XES and discussed in terms of transition cross sections and local densities of states.

Keywords: A. magnetic films and multilayers, E. electron emission spectroscopies.

Recent development in synchrotron radiation sources and instrumentation, the high brightness of third generation sources, has created a growing interest in the use of soft X-ray emission spectroscopy (SXES). Because of site (element) selectivity new research areas in SXES comprise quite diversive phenomena such as atomic and molecular adsorbates on surfaces [1, 2], high temperature superconductors [3, 4], and the study of buried (thin) layers or interfaces [5–7].

As first suggested theoretically by Strange *et al.* [8] measurements of the magnetic circular dichroism in X-ray emission (XE-MCD) for different pure transition metals [9–11] demonstrated that the total non-polarization-resolved emission shows different intensities for opposite relative orientations of the *incident* photon helicity and the sample magnetization. It should be mentioned that also a method to distinguish emitted photons with different helicity is reported [12].

A relativistic spin-polarized one-particle theory of X-ray emission spectroscopy is presented in terms of a multiple scattering formalism which in turn conveniently describes the electronic states for an ensemble of scattering potentials. For the present purpose it is important to emphasize that for each different cell (site) the following Kohn-Sham-Dirac Hamiltonian $\mathcal{H}$ has to be considered [13, 14],

$$\mathcal{H} = c\alpha \cdot p + (\beta - I_4)mc^2 + I_4 V^{\text{eff}}(\mathbf{r}) + \Sigma_z B^{\text{eff}}(\mathbf{r}) \,, \quad (1)$$

where c is the velocity of light, m the mass of the electron, I_n a n-dimensional unit matrix,

$$\alpha = \begin{pmatrix} 0 & \sigma \\ \sigma & 0 \end{pmatrix} \,, \quad \beta = \begin{pmatrix} I_2 & 0 \\ 0 & -I_2 \end{pmatrix} \,, \quad (2)$$

$$\Sigma_z = \begin{pmatrix} \sigma_z & 0 \\ 0 & \sigma_z \end{pmatrix} \,, \quad (3)$$

* E-mail: pw@ws1.cms.tuwien.ac.at

and σ is a vector comprising the usual Pauli-matrices σ_i, $i = x, y, z$. In Eq. (1) spherical symmetry for the effective potential V^{eff} and the effective field B^{eff} is supposed and the local z axis is chosen as axis of quantization. As discussed originally by Feder and Rosicky [15] as well as by Strange *et al.* [16], the eigenfunctions of $\mathcal{H}$ are generally of the following form

$$\psi_Q(\mathbf{r}) = \sum_{Q'} \begin{pmatrix} g_{Q'Q}(r)\ \chi_{Q'}(\hat{r}) \\ i f_{Q'Q}(r)\ \chi_{\overline{Q}'}(\hat{r}) \end{pmatrix}, \tag{4}$$

where $\chi_Q(\hat{r})$ denote spin spherical harmonics [17] with $Q = (\kappa, \mu)$ and $\overline{Q} = (-\kappa, \mu)$. It should be noted that core wavefunctions can be labeled by a well-defined angular momentum index Q, although, according to (4) they are in fact a combination of angular momentum eigenfunctions.

The probability of emission of a photon of energy $\hbar\omega$, momentum $\mathbf{q}$, and a polarization vector $\mathbf{a}_\lambda$ due to an electronic transition from an initial state ψ_i with energy ε_i to a final state ψ_f with energy ε_f is given by first order time-dependent perturbation theory as [18]

$$P_{if}^{q\lambda}(\omega) = \frac{e^2}{2\pi}\, \omega\, \delta(\varepsilon_i - \varepsilon_f - \hbar\omega)\, \left| \left(\mathbf{a}_\lambda^* \cdot \mathbf{j}_{fi}(\mathbf{q}) \right) \right|^2, \tag{5}$$

where in a relativistic formalism the electronic current density matrix element is defined by

$$\mathbf{j}_{fi}(\mathbf{q}) = c\, e \int \psi_f^+(\mathbf{r})\ \alpha\ \psi_i(\mathbf{r})\, e^{-i(\mathbf{q}\cdot\mathbf{r})}\, d^3r, \tag{6}$$

and e is the charge of the electron. It should be recalled that for a given momentum $\mathbf{q}$ the polarization vectors of the two circularly polarized modes, say $\mathbf{a}_+$ (left) and $\mathbf{a}_-$ (right), satisfy the following relations

$$\begin{aligned} &(\mathbf{a}_+^* \cdot \mathbf{a}_+) = (\mathbf{a}_-^* \cdot \mathbf{a}_-) = 1\ , \quad (\mathbf{a}_+^* \cdot \mathbf{a}_-) = 0\ , \\ &(\mathbf{a}_+ \cdot \mathbf{q}) = (\mathbf{a}_- \cdot \mathbf{q}) = 0\,, \end{aligned} \tag{7}$$

which in turn imply that with respect to $\mathbf{q} = q(0, 0, 1)$ the vectors $\mathbf{a}_\pm = \frac{1}{\sqrt{2}}(1, \pm i, 0)$ have to be rotated into the actual direction of the emitted photon. Note also that for photon wavelengths much larger than typical atomic distances the electric dipole approximation, i.e., $e^{-i(\mathbf{q}\cdot\mathbf{r})} = 1$, can be used in Eq. (6).

In a typical X-ray emission process the final state is a well-defined core-state $\psi_{Q_c}(\mathbf{r})$, while all the occupied valences states serve as possible initial states to be summed over,

$$P_f^{q\lambda}(\omega) = \sum_i P_{if}^{q\lambda}(\omega) = \int_{\varepsilon_b}^{\varepsilon_F} d\varepsilon \delta(\varepsilon - \varepsilon_{Q_c} - \hbar\omega) I_{Q_c}^{q\lambda}(\varepsilon), \tag{8}$$

where ε_b is the valence-band bottom, ε_F is the Fermi level, and ε_{Q_c} denotes the energy of a particular core-state. Thus, one obtains for the transition intensity $I_{Q_c}^{q\lambda}(\varepsilon)$ (see also Ref. [19])

$$\begin{aligned} I_{Q_c}^{q\lambda}(\varepsilon) \sim (\varepsilon - \varepsilon_{Q_c}) \iint d^3r\, d^3r'\, \psi_{Q_c}^+(\mathbf{r})\, (\alpha \cdot \mathbf{a}_\lambda^*) \\ \times \operatorname{Im} G(\mathbf{r}, \mathbf{r}'; \varepsilon)\, (\alpha \cdot \mathbf{a}_\lambda)\, \psi_{Q_c}(\mathbf{r}'). \end{aligned} \tag{9}$$

By expressing within multiple scattering theory [20,21] the imaginary part of the one-electron Green's function as

$$\operatorname{Im} G(\mathbf{r}, \mathbf{r}'; \varepsilon) = \sum_{Q_1, Q_2} Z_{Q_1}^n(\mathbf{r}_n; \varepsilon) \operatorname{Im} \tau_{Q_1 Q_2}^{nn}(\varepsilon) Z_{Q_2}^n(\mathbf{r}_n'; \varepsilon)^+ \tag{10}$$

$$\mathbf{r}_n \equiv \mathbf{r} - \mathbf{R}_n\,, \quad \mathbf{r}_n' \equiv \mathbf{r}' - \mathbf{R}_n\,,$$

where n labels the site $\mathbf{R}_n$ of a particular core-state, $Z_Q^n(\mathbf{r}_n; \varepsilon)$ is a properly normalized regular scattering solution, and the $\tau_{Q_1 Q_2}^{nn}(\varepsilon)$ denote matrix elements of the scattering path operator, Eq. (9) can be rewritten as a sum over all relevant sites,

$$I_{Q_c}^{q\lambda}(\varepsilon) = \sum_n I_{Q_c}^{q\lambda n}(\varepsilon)\,. \tag{11}$$

In the case of a simple threedimensional lattice Eq. (11) reduces to

$$I_{Q_c}^{q\lambda}(\varepsilon) = I_{Q_c}^{q\lambda 0}(\varepsilon) |T^{(3)}|\,, \tag{12}$$

where $I_{Q_c}^{q\lambda 0}(\varepsilon)$ denotes the contribution to the total intensity per unit cell. In the case of a system characterized by a simple twodimensional lattice, see e.g. Ref. [22], Eq. (11) can be written as

$$I_{Q_c}^{q\lambda}(\varepsilon) = \sum_{i=1}^{N} I_{Q_c}^{q\lambda(i0)}(\varepsilon) |T^{(2)}|\,, \tag{13}$$

where $I_{Q_c}^{q\lambda(i0)}(\varepsilon)$ refers to the contribution from the unit cell in layer i and N is the total number of layers to be considered. The factor $|T^{(n)}|$ in Eqs. (12) and (13) corresponds to the respective order of the translation group. Clearly enough by considering only unit-cell-like contributions, the factor $|T^{(n)}|$ can be omitted. It should be noted that because of the large escape length λ of photons for XES no exponential escape factor of the form $\exp(-d_i/\lambda)$, where d_i measures the distance of the i-th layer from the surface, has to be considered.

Using Eqs. (9)–(11) the transition intensity at a given site n is defined as

$$\begin{aligned} I_{Q_c}^{q\lambda n}(\varepsilon) \sim (\varepsilon - \varepsilon_{Q_c}) \\ \times \sum_{Q_1, Q_2} \mathcal{M}_{Q_1}^{q\lambda n}(\varepsilon)^* \operatorname{Im} \tau_{Q_1 Q_2}^{nn}(\varepsilon) \mathcal{M}_{Q_2}^{q\lambda n}(\varepsilon)\,, \end{aligned} \tag{14}$$

with

$$\mathcal{M}_Q^{q\lambda n}(\varepsilon) = \int d^3r_n Z_Q^n(\mathbf{r}_n;\varepsilon)^+ (\alpha \cdot \mathbf{a}_\lambda)\, \psi_{Q_c}(\mathbf{r}_n)\,. \quad (15)$$

The matrix elements $\mathcal{M}_Q^{q\lambda n}(\varepsilon)$ can easily be evaluated using the method described by Ebert [23]. In order to link the local partial densities of states (LDOS) $n_Q^n(\varepsilon)$,

$$n_Q^n(\varepsilon) = -\frac{1}{\pi}\sum_{Q'} R_{QQ'}^n(\varepsilon)\,\mathrm{Im}\tau_{Q'Q}^{nn}\,, \quad (16)$$

$$R_{QQ'}^n(\varepsilon) \equiv \int d^3r_n Z_Q^n(\mathbf{r}_n;\varepsilon)^+ Z_{Q'}^n(\mathbf{r}_n;\varepsilon)\,, \quad (17)$$

to the calculated intensities, throughout this work the following approximation is used

$$I_{Q_c}^{q\lambda n}(\varepsilon) \sim (\varepsilon - \varepsilon_{Q_c}) \sum_Q \sigma_Q^{q\lambda n}(\varepsilon) n_Q(\varepsilon)\,, \quad (18)$$

where the so-called transition cross-sections $\sigma_Q^{q\lambda}(\varepsilon)$ are given by

$$\sigma_Q^{q\lambda n}(\varepsilon) = |\mathcal{M}_Q^{q\lambda n}(\varepsilon)|^2 / R_{QQ}^n(\varepsilon)\,. \quad (19)$$

In several cases we checked numerically that Eq. (18) is indeed a very good approximation to the more exact form in Eq. (14).

Obviously, in non-magnetic materials the *lcp* and *rcp* emission intensities are identical. For magnetic materials, however, the *lcp*- and *rcp* spectra are different due to the combined action of spin-polarization and spin-orbit coupling: if the direction of the emitted photon is parallel to the orientation of the magnetization dichroism reaches a maximum, while for a perpendicular arrangement it vanishes. Thus, in principle, by monitoring the emission intensity in various directions it is possible to determine locally the orientation of the magnetization.

1. RESULTS

In the following we show results for the L_3-XES intensities of a Co monolayer on a Cu(100) substrate as capped by different $3d$, $4d$, and $5d$ transition metals. Details of the electronic and magnetic structure of these materials can be found in Ref. [24]. All calculated spectra are broadened with a Gaussian (finite spectrometer resolution) and a Lorentzian (lifetime effects) function. Here, we used a core-state broadening of 0.3 eV, a valence-band lifetime broadening of 0.3 eV and a spectrometer resolution of 0.5 eV.

In Fig. 1 the local densities of states (LDOS) of the Co monolayer capped by a monolayer of Co, Au, Ru, Ir, or Os are shown. In addition to the total LDOS,

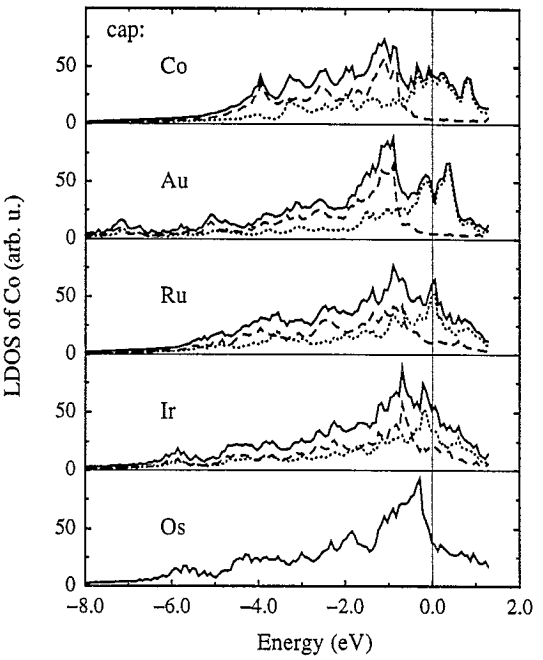

Fig. 1. Local densities of states of a Co monolayer on Cu(100) for different cap layers. In addition to the total DOS (solid curves) also the majority-spin part (dashed lines) and the minority-spin part (dotted lines) are shown. It should be noted that a Co monolayer capped by Os is paramagnetic.

Table 1. Energies and spin characters of the 2p core levels of Co capped by Au

κ_c	μ_c	ε_{Q_c} (eV)	S_{Q_c}
-2	-3/2	-757.262	-0.50
-2	-1/2	-757.491	-0.21
-2	+1/2	-757.728	0.12
-2	+3/2	-757.972	0.50
1	+1/2	-772.297	-0.12
1	-1/2	-772.527	0.21

also spin-resolved contributions ($s = \frac{1}{2}$: majority spins, $s = -\frac{1}{2}$: minority spins) are plotted, subduced from a transformation of the $(\kappa\mu)$ representation of the LDOS to a (lms) representation (see Ref. [20]). Since for valence states of predominantly Co character the spin–orbit coupling is rather small, such a representation is quite adequate in tracing changes in these states whith respect to different caps. Evidently, for a decreasing magnetic moment of Co (see Table 2) one finds a transfer of minority-spin states from above the Fermi level to occupied states and vice versa for the majority-spin DOS. This kind of changes in the spin-polarized DOS are discussed below in terms of *lcp* and *rcp* XES.

Not shown in here, but quite obviously, the largest cross-sections are for d-like electrons ($l = 2$). It is interesting to note that the selection rule $\mu_c = m + s \pm 1$

Table 2. Magnetic moments of the Co atoms for different cap materials as determined from electronic structure calculations [24] and from the dichroism spectra as normalized to CoCo/Cu(100)

cap	m_{KKR} (μ_B)	m_{XES} (μ_B)
Co	1.74	1.74
Au	1.55	1.48
Ru	1.1	1.22
Ir	0.65	0.64
Os	0	0

(see Ref. [23]) generally allows a coupling of the core-states to valence states of different spin. The core level energies ε_{Q_c} and the spin character S_{Q_c},

$$S_{Q_c} = \frac{1}{2}\int \psi^+_{Q_c}(\mathbf{r})\, \beta\Sigma_z\, \psi_{Q_c}(\mathbf{r})d\mathbf{r}\,, \qquad (20)$$

of the $2p_{3/2}$ Co core states are shown in Table 1. Since the core states for $\mu_c = \pm 1/2$ are of mixed spin character, the cross sections for transitions from majority and from minority valence states have comparable magnitudes. In terms of the photon helicity the dominating cross sections for $\mu_c = -3/2$ refer to *lcp* emission, while for $\mu_c = +3/2$ they are related to *rcp* like photons. Considering the different shapes of the majority and minority LDOS's, this particular cross-section effect apparently gives rise to dichroism in the calculated XES intensity. Since especially the cross-sections for $\mu_c = \pm 3/2$ are fairly insensitive to changes of the spin-polarization of the Co layer with respect to different cap materials, the changes in the spectra due to different cap materials can be explained predominantly by differences in the LDOS's shown in Fig. 1.

As shown in Figs 2(a and b) the polarization-resolved X-ray emission spectra of each of the Zeeman split (μ-resolved) $2p_{3/2}$ core levels of Co in the system AuCo/Cu(100) directly map the LDOS's via the cross-sections discussed above. The dominating $\mu_c = 3/2$ and $\mu_c = 1/2$ *rcp* spectra are governed by majority valence states with a corresponding maximum at about -1 eV, while the minority valence states contribute mostly to the $\mu_c = -3/2$ and $\mu_c = -1/2$ *lcp* spectra with a maximum near the Fermi level. The relative height of the individual spectra corresponds to the strength of the angular momentum part of the matrix elements as discussed also in the context of X-ray absorption [25,26]. Since the minority states above ε_F do not contribute to the spectra, the *rcp* intensity is more pronounced than the *lcp* intensity. This is apparent also from the total *lcp* and *rcp* L_3 spectra shown in Figs 2(c and d). Here, the sums over the four μ-resolved L_3 spectra (dashed lines) are compared with the emitted intensities (solid curves) including the effect of Zeeman splitting of the core states (see Table 1). It should be noted that the maximum splitting (0.71 eV) is between the $\mu_c = -3/2$ and the $\mu_c = +3/2$ core-states, namely the ones with the largest cross-sections and emission intensities. In particular, in the emission spectrum the contributions corresponding to core levels with higher energies ($\mu_c = -3/2, -1/2,$ and $+1/2$) are shifted with respect to the lowest level ($\mu_c = +3/2$). As can be seen from Fig. 2 this leads to a dominate shift of the *lcp* intensity $I^+(\varepsilon)$, while the largest peak in the *rcp* intensity $I^-(\varepsilon)$ remains nearly unchanged. Thus, the large minority LDOS at the Fermi energy is not seen directly in the L_3 X-ray emission spectrum, even by analyzing photons of different polarization. Consequently, for magnetic systems the traditional statement that the spectral intensity maps the DOS of the occupied states has to be applied very cautiously: the Zeeman splitting for the Co $2p_{3/2}$ core levels is already of the same order of magnitude as the present spectrometer resolution.

The L_3 emission spectra of Co for systems with a Co, Au, Ru, or Ir cap layer are shown in Fig. 3. When comparing the cases of a Ru, Ir, and Au cap with that of a Co cap (see also Fig. 1) the hybridization of the Co states with the cap states can be seen as a broadening of the spectra. The change of spin polarization in the Co layer, however, clearly shows up in variations of the *lcp* and *rcp* spectra. Both the difference of the maxima and the energetical shift of $I^+(\varepsilon)$ and $I^-(\varepsilon)$ decrease with a decreasing Co moment. It is interesting to note that these changes are only very weakly reflected in the total spectra.

Finally, by assuming that the *lcp* and the *rcp* spectra mainly comprise contributions of spin-up and spin-down valence states, respectively, an attempt can be made to correlate the dichroism to the magnetic (spin-only) moment of Co by means of the following integral

$$m_{XES} = \int_{\varepsilon_b}^{\varepsilon_F} [I^-(\varepsilon) - I^+(\varepsilon)]\, d\varepsilon\,. \qquad (21)$$

This procedure can be related to the use of sum rules in MCD from X-ray absorption [23]. Indeed, neglecting the so-called orbital moment of Co the spin moment becomes proportional to the integrated L_3 dichroism spectrum. As a reference we normalized these values to the magnetic moment of a Co layer with a cap of an additional Co layer. In Table 2 these 'spectroscopically' determined magnetic moments m_{XES} are compared with those obtained from selfconsistent electronic structure calculations [24]. As can be seen, corresponding values differ within about 10 %. These deviations directly show the influence of the energy-dependent transition matrix elements and the spin-channel mixing as follows from a relativistic treatment of X-ray emission.

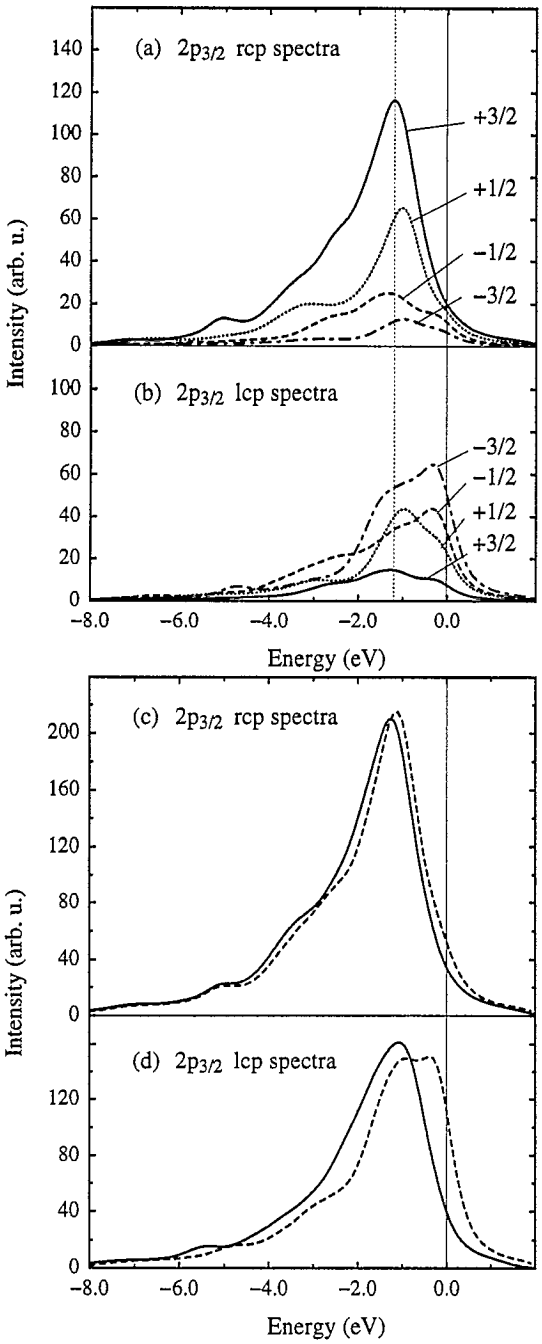

Fig. 2. X-ray emission *rcp* and *lcp* L_3 spectra of a Co monolayer in the AuCo/Cu(100) system. In (a) and (b) the individual contributions with respect to the Zeeman split $2p_{3/2}$ core states are shown. In (c) and (d) the full lines refer to their sums, whereas the dashed lines refer to a sum with respect to a common (κ = -2, μ = +3/2) energy reference level.

We have shown the changes in the L_3 X-ray emission spectra of a buried Co layer capped by several transition metals. According to the variations in the Co magnetization with respect to the cap material the main peak in the total XE spectra is shifted. Furthermore, depending on the type of the cap characteristic hybridization effects of the Co layer with the cap layer show a loss or gain of emission intensity in different energy ranges. The magnetic dichroism spectra are especially sensitive to different caps. Analyzing the photon polarizations we find magnetic asymmetry ratios up to 30% caused by both the large spin polarization in the valence band and the 'spin-orbit coupling' for the core states. For comparison, in valence-band photoemission from a thin Co film on Cu the magnetic dichroism reaches only 4% [27] reflecting the considerably weaker 'spin-orbit coupling' in the 3*d* band. Furthermore, the influence of the Zeeman split core states was clearly demonstrated. The present paper proves that XES can be a very valuable tool in describing the electronic structure of magnetic multilayers, in particular, with buried interfaces.

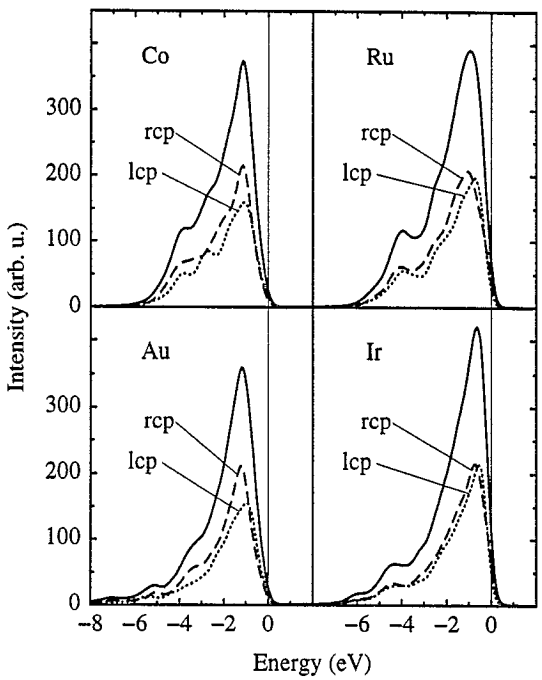

Fig. 3. X-ray emission L_3 spectra of Co/Cu(100) with a Co, Au, Ru, and Ir cap. The *rcp* (dashed lines) and *lcp* (dotted lines) emission intensities are shown together with their sum (solid lines).

Acknowledgements—Financial support was provided by the TMR network on "*Ab-initio* calculations of magnetic properties of surfaces, interfaces, and multilayers" (contract No.: EMRX-CT96-0089), the Center of Computational Materials Science (contract No.: GZ 308.941/2-IV/95) and the Hungarian National Science Foundation (OTKA T24137 and T21228).

REFERENCES

1. Wiell, T., *et al., Surf. Sci. Lett.*, **304**, 1994, L451.
2. Wassdahl, N., Nilsson, A., Wiell, T., Tillborg, H., Duda, L.-C., Guo, H., Martensson, N. and Nordgren, J., *Phys. Rev. Lett.*, **69**, 1992, 812.
3. Butorin, S.M., *et al., Phys. Rev. B,* **51**, 1995, 11915.
4. Guo, J.-H., Butorin, S.M., Wassdahl, N., Skytt, P. and Nordgren, J., *Phys. Rev. B,* **49**, 1994, 1376.
5. Nilsson, P.O., Kanski, J., Thordson, J.V., Andersson, T. G., Nordgren, J., Guo, J. and Magnusson, M., *Phys. Rev. B,* **52**, 1995, R8643.
6. Carlisle, J., *et al., Appl. Phys. Lett.*, **67**, 1995, 34.
7. Nilsson, A., Stöhr, J., Wiell, T., Alden, M., Bennich, P., Wassdahl, M.G., Samant, S.S.P., Parkin, N., Martensson, J., Nordgren, B., Johansson, N. and Skriver, H.L., *Phys. Rev. B,* **54**, 1996, 2917.
8. Strange, P., Durham, P.J. and Györffy, B.L., *Phys. Rev. Lett.*, **67**, 1991, 3590.
9. Hague, C.F., Mariot, J.-M., Strange, P., Durham, P.J. and Györffy, B.L., *Phys. Rev. Lett.*, **48**, 1993, 3560.
10. Duda, L.-C., Stöhr, J., Mancini, D.C., Nilsson, A., Samant, M.G., Wassdahl, N. and Nordgren, J., *Vacuum,* **46**, 1995, 1125.
11. Duda, L.-C., Stöhr, J., Mancini, D.C., Nilsson, A., Wassdahl, N., Nordgren, J. and Samant, M.G., *Phys. Rev. B,* **50**, 1994, 16758.
12. Kuiper, P., Duda, L.-C., Mancini, D.C. and Nordgren, J., Annual Report MAXLAB, Lund, 1993.
13. MacDonald, A.H. and Vosko, S.H., *J. Phys.: Solid State Phys.*, **12**, 1979, 2977.
14. Ramana, M.V. and Rajagopal, A.K., *Adv. Chem. Phys.*, **54**, 1983, 231.
15. Feder, R. and Rosicky, F., *Z. Phys. B,* **52**, 1983, 52.
16. Strange, P., Staunton, J. and Györffy, B.L., *J. Phys. C,***17**, 1984, 3355.
17. Rose, M.E., *Relativistic Electron Theory* (New York: Wiley, 1961).
18. Berestetzki, W.B., Lifshitz, E.M. and Pitajevski, L.P., Relativistic Quantum Theory (eds. Landau, L.D. and Lifshitz, E.M., in *Course of Theoretical Physics*, Vol. IV., Oxford: Pergamon, 1971).
19. Durham, P.J., *The Electronic Structure of Complex Systems*, (eds. P. Phariseau and W.M. Temmerman, New York: Plenum, 1984), p. 709.
20. Staunton, J., Györffy, B.L. and Weinberger, P., *J. Phys. F,* **10**, 1980, 2665.
21. Weinberger, P., *Electron scattering Theory for Ordered and Disordered Matter* (Clarendon, Oxford, 1990).
22. Weinberger, P., *Phil. Mag. B*, **75**, 1997, 509.
23. Ebert, H., *Rep. Prog. Phys.*, **59**, 1996, 1665.
24. Szunyogh, L., Újfalussy, B., Pustogowa, U. and Weinberger, P., *Phys. Rev. B,* **57**, 1998, 8838.
25. Ebert, H., Baumgarten, L., Schneider, C.M. and Kirschner, J., *Phys. Rev. B,* **44**, 1991, 4406.
26. Ebert, H. and Guo, G.-Y., *Solid State Comm.*, **91**, 1994, 85.
27. Venus, D., Kuch, W., Dittschar, A., Zharnikov, M., Schneider, C.M. and Kirschner, J., *Phys. Rev. B,* **52**, 1995, 6174.